

Citation for published version:

Maria Dimitriadi, et al, 'Decreased function of survival motor neuron protein impairs endocytic pathways', *PNAS*, Vol. 113(30): E4377-E4386, July 2016.

DOI:

<https://doi.org/10.1073/pnas.1600015113>

Document Version:

This is the Accepted Manuscript version.

The version in the University of Hertfordshire Research Archive may differ from the final published version.

Copyright and Reuse:

© 2016 PNAS

Content in the UH Research Archive is made available for personal research, educational, and non-commercial purposes only. Unless otherwise stated, all content is protected by copyright, and in the absence of an open license, permissions for further re-use should be sought from the publisher, the author, or other copyright holder.

Enquiries

If you believe this document infringes copyright, please contact the Research & Scholarly Communications Team at rsc@herts.ac.uk

Decreased Function of Survival Motor Neuron Protein Impairs Endocytic Pathways

Maria Dimitriadi^{a,b}, Aaron Derdowski^{c*}, Geetika Kalloo^{a*}, Melissa S. Maginnis^{c,d}, Patrick O' Hern^a, Bryn Bliska^a, Altar Sorkaç^a, Ken C.Q. Nguyen^e, Steven J. Cook^e, George Pouligiannis^f, Walter J Atwood^c, David H. Hall^e, Anne C. Hart^a

^aDepartment of Neuroscience, Brown University, Providence, RI 02912, USA; ^bDepartment of Biological and Environmental Sciences, University of Hertfordshire, Hatfield, AL10 9AB, UK; ^cDepartment of Molecular Biology, Cell Biology and Biochemistry, Brown University, Providence, RI 02912, USA; ^dDepartment of Molecular and Biomedical Sciences, University of Maine, Orono, ME 04469, USA, ^eDominick P. Purpura Department of Neuroscience, Albert Einstein College of Medicine, Bronx, NY 10461, USA; ^fThe Institute of Cancer Research, 237 Fulham Road, Chester Beatty Labs, London, SW3 6JB, UK. *These two authors contributed equally and are listed in alphabetical order.

Submitted to Proceedings of the National Academy of Sciences of the United States of America

Spinal Muscular Atrophy (SMA) is caused by depletion of the ubiquitously expressed survival motor neuron (SMN) protein, with one in forty Caucasians being heterozygous for a disease allele. SMN is critical for the assembly of numerous ribonucleoprotein complexes, yet, it is still unclear how reduced SMN levels affect motor neuron function. Here, we examined the impact of SMN depletion in *Caenorhabditis elegans* and found that decreased function of the SMN ortholog SMN-1 perturbed endocytic pathways at motor neuron synapses and in other tissues. Diminished SMN-1 levels caused defects in *C. elegans* neuromuscular function and *smn-1* genetic interactions were consistent with an endocytic defect. Changes were observed in synaptic endocytic proteins when SMN-1 levels decreased. At the ultrastructural level, defects were observed in endosomal compartments, including significantly fewer docked synaptic vesicles. Finally, endocytosis-dependent infection by JC polyomavirus (JCPyV) was reduced in human cells with decreased SMN levels. Collectively, these results demonstrate for the first time that SMN depletion causes defects in endosomal trafficking that impair synaptic function, even in the absence of motor neuron cell death.

endocytic trafficking | survival motor neuron | spinal muscular atrophy | *C. elegans* | infection

Introduction

Spinal Muscular Atrophy (SMA) is one of the most severe neuromuscular diseases of childhood, with an incidence of 1 in 10,000 live births and a high carrier frequency of roughly 1 in 40 Caucasians (1-3). SMA is caused by reduced levels of the ubiquitously expressed survival of motor neuron (SMN) protein and results in degeneration of α -spinal cord motor neurons, muscle weakness, and/or death. Two human genes encode the SMN protein, *SMN1* and *SMN2*. SMA alleles arise at relatively high frequency due to small intrachromosomal *de novo* rearrangements including the *SMN1* locus (4). Patients often carry homozygous *SMN1* deletions, although missense and nonsense alleles exist (5). Multiple copies of *SMN2* rarely compensate for loss of *SMN1* due to a C>T nucleotide change in *SMN2* exon 7 that perturbs pre-mRNA splicing and results in a truncated protein of diminished function and stability (SMN ^{Δ 7}) (5-9).

SMN has numerous roles and interacts with various proteins; yet, it remains unclear which interactions are most pertinent to SMA pathogenesis. As a component of the Gemin complex, SMN is required for biogenesis of small nuclear ribonucleoprotein (snRNP) particles critical for pre-mRNA splicing (10-12). Furthermore, SMN is needed for stress granule formation (13, 14), is found in RNP granules moving through neuronal processes, and is part of RNP complexes implicated in synaptic local translation (15-20). Additional roles for SMN, in transcription (21), in the PTEN-mediated protein synthesis pathway (22), in translational control (23) and in cell proliferation/differentiation (24) have been described. Importantly, no consensus has been reached

regarding the cellular and molecular pathways whose perturbation results in SMA pathology. Identifying the cellular pathways most sensitive to decreased SMN is essential to understand how SMN depletion causes neuronal dysfunction/death in SMA and to accelerate therapy development.

One of the early events in SMA pathogenesis is the loss of neuromuscular junction (NMJ) function, evidenced by muscle denervation, neurofilament accumulation, and delayed neuromuscular maturation (25-27). In addition, reduced neurotransmitter release and decreased numbers of docked vesicles that precede axonal degeneration and/or motor neuron death have been reported at synapses of severe SMA mouse models (28, 29). Notably, accumulation of synaptic vesicles away from release sites was observed in SMA fetal samples (30). The proximate cause of these synaptic changes is unclear. Numerous hypotheses have been proposed, including functional abnormalities in axonal transport and/or calcium channel loss in the nerve terminals (25-30), but none have explained the defects observed in SMA presynaptic regions.

Here, we use a previously established model of SMA in the nematode *Caenorhabditis elegans* (*C. elegans*) and show, using functional assays, pharmacological challenges, and genetic epistasis, that decreased SMN levels cause endocytic pathway defects. In *C. elegans* cholinergic motor neurons, decreased SMN levels caused aberrant localization of proteins critical for endocytosis.

Significance

Spinal Muscular Atrophy (SMA) is a devastating motor neuron disease, caused by decreased levels of the ubiquitous Survival Motor Neuron (SMN) protein. Despite the well-characterized role of SMN in pre-mRNA splicing, it remains unclear why SMA has a high carrier frequency (~1:50 Caucasians) and why diminished SMN affects synaptic function. Here, we demonstrated for the first time that SMN depletion causes defects in endosomal trafficking that impair synaptic function. Additionally, diminished SMN in human cells reduced endocytosis-dependent viral infection. It is possible that decreased SMN function may increase resistance to infection. Our findings point to endocytic trafficking as a major player in SMA pathogenesis.

Reserved for Publication Footnotes

137
138
139
140
141
142
143
144
145
146
147
148
149
150
151
152
153
154
155
156
157
158
159
160
161
162
163
164
165
166
167
168
169
170
171
172
173
174
175
176
177
178
179
180
181
182
183
184
185
186
187
188
189
190
191
192
193
194
195
196
197
198
199
200
201
202
203
204

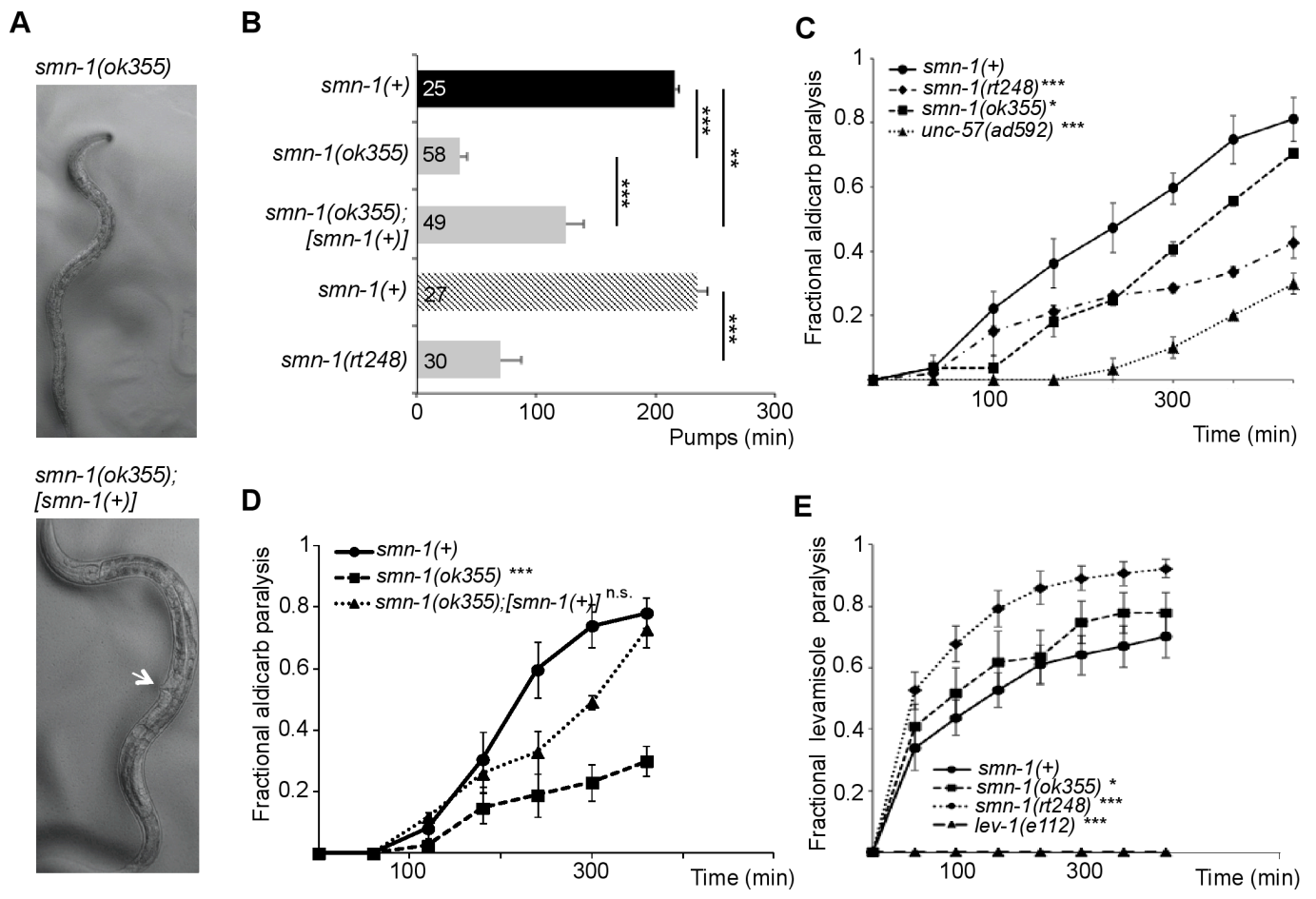


Fig. 1. Decreased SMN function in *C. elegans* causes defective motor neuron function. (A) Images of age-matched *smn-1(ok355)* (top) and *smn-1(ok355);[smn-1(+)]* (bottom) animals. Single-copy insertion of an *[smn-1(+)]* transgene *rtSi10* rescued *smn-1(ok355)* larval lethality and growth, but did not restore fertility. Arrow indicates adult vulva, which has not developed in age matched *smn-1(ok355)*. (B) *smn-1(ok355)* and *smn-1(rt248)* animals had reduced pumping rates versus respective *smn-1(+)* controls. Studies in panel B involving *smn-1(ok355)* were run independently from studies with *smn-1(rt248)*, but combined into one panel for brevity (black column: *smn-1(+)* control for *ok355*; cross-hatched: *smn-1(+)* control for *rt248*). *smn-1(ok355)* pharyngeal pumping defects (at day 3 post-hatching) were ameliorated by introducing an *smn-1(+)* rescue construct. Mean \pm SEM; Mann-Whitney *U*-test, two tailed: ***p* < 0.01, ****p* < 0.001. (C) *smn-1(ok355)* and *smn-1(rt248)* animals were resistant to the acetylcholinesterase inhibitor alicarb. Time course for paralysis induced by 1 mM alicarb in *smn-1(+)*, *smn-1(ok355)*, *smn-1(rt248)* and *unc-57(ad592)* young L4 hermaphrodites is shown. *unc-57* encodes *C. elegans* endophilin A; *unc-57(ad592)* causes inappropriate resistance to alicarb (43). Log-rank test: **p* < 0.05, ****p* < 0.001. (D) The alicarb resistance of *smn-1(ok355)* animals was mostly restored by *[smn-1(+)]* genomic rescue (*rtSi10*). Log-rank test: ****p* < 0.001, n.s., not significant. (E) *smn-1(ok355)* and *smn-1(rt248)* were hypersensitive to levamisole, a nicotinic ACh receptor agonist. *smn-1(+)*, *smn-1(ok355)*, *smn-1(rt248)* and *lev-1(e211)* young L4 hermaphrodite paralysis on 0.4 mM levamisole plates is reported. *lev-1(e211)* animals lack a nicotinic ACh receptor subunit. Error bars indicate \pm SEM. Log-rank test: **p* < 0.05, ****p* < 0.001, n.s., not significant.

Further, ultrastructural analysis of endosomal compartments revealed numerous defects when SMN levels were depleted, including loss of synaptic docked vesicles. Endocytic pathway defects were also observed in non-neuronal tissues. Finally, endocytosis-dependent infection by JC polyomavirus (JCPyV) was reduced in human cells with decreased SMN levels. Combined, these results demonstrate for the first time that SMN depletion causes widespread defects in endosomal trafficking that impair synaptic function in motor neurons, even in the absence of motor neuron death.

Results

***smn-1* is required for neuromuscular function.** The *C. elegans* genome harbors a single ortholog of SMN, SMN-1. Animals with a wild type copy of the endogenous *smn-1* gene are referred to herein as *smn-1(+)* and are used as controls. Diminished *smn-1* function causes slow growth, larval lethality and impairs neuromuscular function in pharyngeal pumping during feeding (31, 32) (Figure 1A). *C. elegans* feed on microorganisms using a discrete subset of muscles and neurons in the pharynx (33).

Animals pump symmetrically and continuously roughly 250 times per minute when food is present. The pumping rates of *smn-1* loss of function animals (*smn-1(ok355)*) are significantly reduced (*p* = 3e-12, Figure 1B) (31, 32). To confirm that the defects described here are caused by *smn-1* loss, we generated a new *smn-1* allele, *smn-1(rt248)*, using CRISPR/Cas9 targeted mutagenesis (34, 35). The *rt248* allele results in a premature truncation at the 19th amino acid (D19fs) of the SMN-1 protein, disrupts RNA binding, Tudor and oligomerization domains, and likely eliminates SMN-1 protein function (Figure S1). The pumping rates of *smn-1(rt248)* animals were significantly reduced (*p* = 3e-9, Figure 1B). This defect was re-confirmed using RNA interference (*smn-1(RNAi)*), *p* = 2e-09, Figure S2). These neuromuscular defects are progressive and not a developmental process; homozygous *smn-1(ok355)* and *smn-1(rt248)* larvae initially resemble wild type animals due to maternal *smn-1* loading. Eventually, homozygous *smn-1* animals lose maternally-loaded *smn-1* product, suffer decreased motor neuron function, and usually die as larvae. However, no motor neuron loss is observed (36). The impact of *smn-1* loss is recessive; heterozygous animals are overtly normal. Single copy insertion

205
206
207
208
209
210
211
212
213
214
215
216
217
218
219
220
221
222
223
224
225
226
227
228
229
230
231
232
233
234
235
236
237
238
239
240
241
242
243
244
245
246
247
248
249
250
251
252
253
254
255
256
257
258
259
260
261
262
263
264
265
266
267
268
269
270
271
272

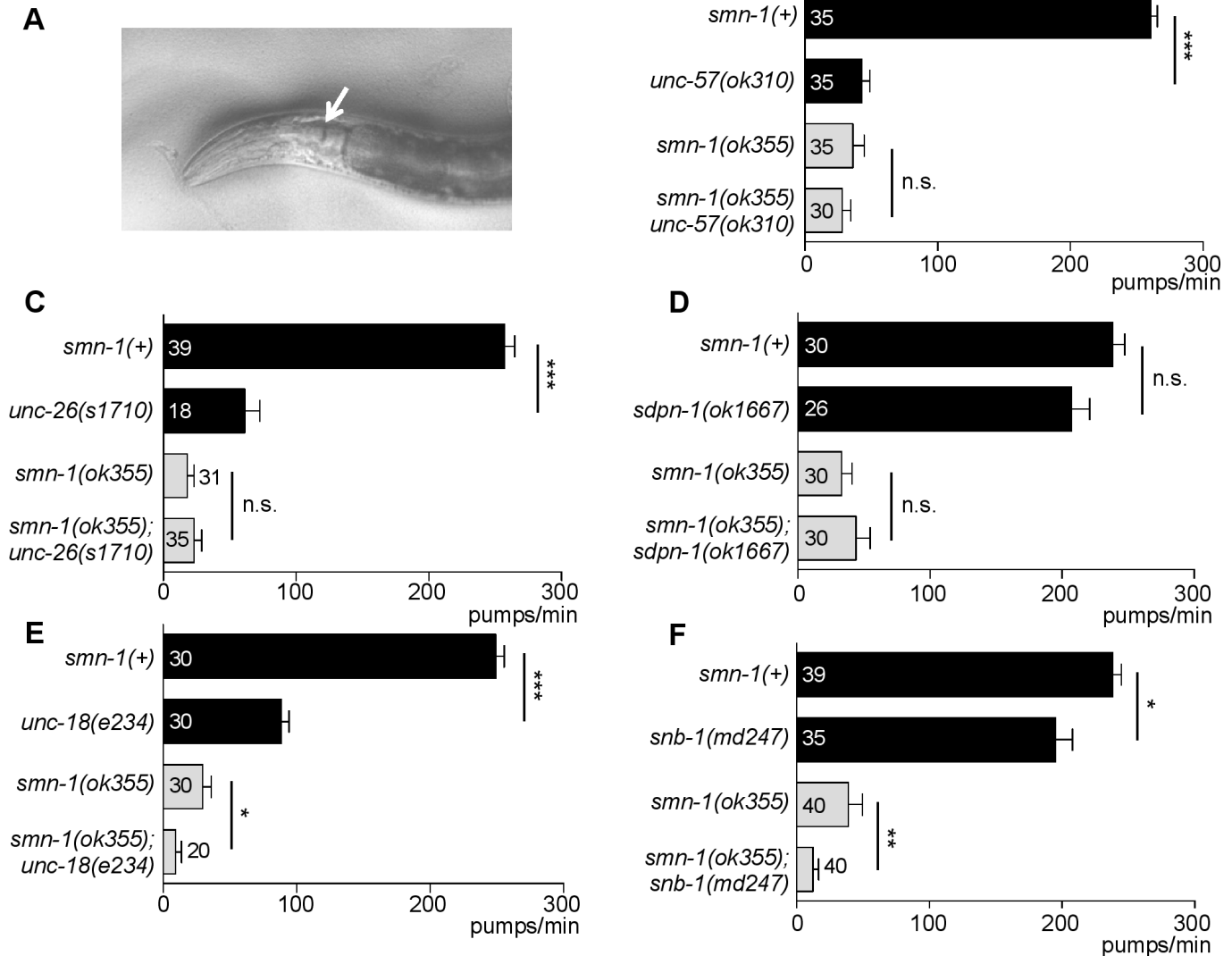
273
274
275
276
277
278
279
280
281
282
283
284
285
286
287
288
289
290
291
292
293
294
295
296
297
298
299
300
301
302
303
304
305
306
307
308
309
310
311
312
313
314
315
316
317
318
319
320
321
322
323
324
325
326
327
328
329
330
331
332
333
334
335
336
337
338
339
340

Fig. 2. Double mutant analysis using pharyngeal pumping suggests synaptic vesicle recycling defects. (A) *C. elegans* neuromuscular function is assessed as pharyngeal grinder (arrow) movement during feeding. (B-D) Complete loss of endophilin-A, synaptojanin, or syndapin (*unc-57(ok310)*, *unc-26(s1710)*, or *sdpn-1(ok1667)*) did not alter *smn-1(ok355)* pharyngeal pumping defects. (E and F) Complete loss of Munc-18 or synaptobrevin (*unc-18(e234)* or *snb-1(md247)*) exacerbated *smn-1(ok355)* pharyngeal pumping defects. Additive defects with SV exocytosis loss of function mutants suggested that SMN-1 depletion impairs the SV recycling pathway. Total number of animals tested listed for each genotype \pm SEM; Mann-Whitney *U*-test, two tailed: * $p < 0.05$, ** $p < 0.01$, *** $p < 0.001$, n.s., not significant.

of an *smn-1(+)* genomic DNA transgene (containing 445 bp of 5' regulatory sequences, 816 bp *smn-1* genomic DNA and 558 bp of 3' non-coding sequences, called *rtSi10*) fully rescued larval lethality, partially ameliorated pharyngeal pumping defects ($p = 0.0004$, Figures 1A and 1B), but did not restore fertility of *smn-1(ok355)* animals. The partial rescue of *smn-1(ok355)* defects may arise from regulatory sequences required for SMN-1 expression that were not included in the rescue construct. Nevertheless, the results presented here confirm that these defects can be attributed to SMN-1 depletion and that SMN-1 is required for normal neuromuscular function.

***smn-1* regulates synaptic transmission.** Studies in SMA patients and mice revealed defects in motor neuron synapses when SMN levels are reduced (37). We examined motor neuron function pharmacologically in *smn-1(ok355)* and *smn-1(rt248)* animals by assessing sensitivity to aldicarb and levamisole. Aldicarb is an acetylcholinesterase inhibitor that causes muscle hypercontraction and paralysis due to accumulation of acetylcholine (ACh) in the synaptic cleft (38). Decreased ACh release slows

the onset of aldicarb-induced paralysis. We found that *smn-1(ok355)* and *smn-1(rt248)* animals were resistant to aldicarb compared to animals with normal *smn-1* function ($p = 0.03$ *smn-1(ok355)* and $p = 8e-6$ *smn-1(rt248)* vs *smn-1(+)* derived from *+/hT2* parents, Figure 1C). This increased resistance was due to diminished *smn-1* as introducing an *smn-1(+)* genomic DNA fragment restored aldicarb sensitivity ($p = 0.17$, Figure 1D). Resistance to aldicarb was also observed when *smn-1* was knocked down by RNAi specifically in cholinergic neurons ($p = 0.004$, Figure S3) (39). Therefore, SMN-1 is required for neuromuscular function, likely in cholinergic neurons, which is consistent with a previous study reporting resistance to the acetylcholinesterase inhibitor pyridostigmine bromide (40). *smn-1(ok355)* and *smn-1(rt248)* aldicarb resistance could be caused by decreased neurotransmitter release or reduced post-synaptic response to acetylcholine. To discriminate, we assessed *smn-1(ok355)* and *smn-1(rt248)* sensitivity to levamisole, an agonist, which induces paralysis by directly activating post-synaptic nicotinic receptors. Levamisole resistance is thought to be purely post-synaptic (41). *smn-*

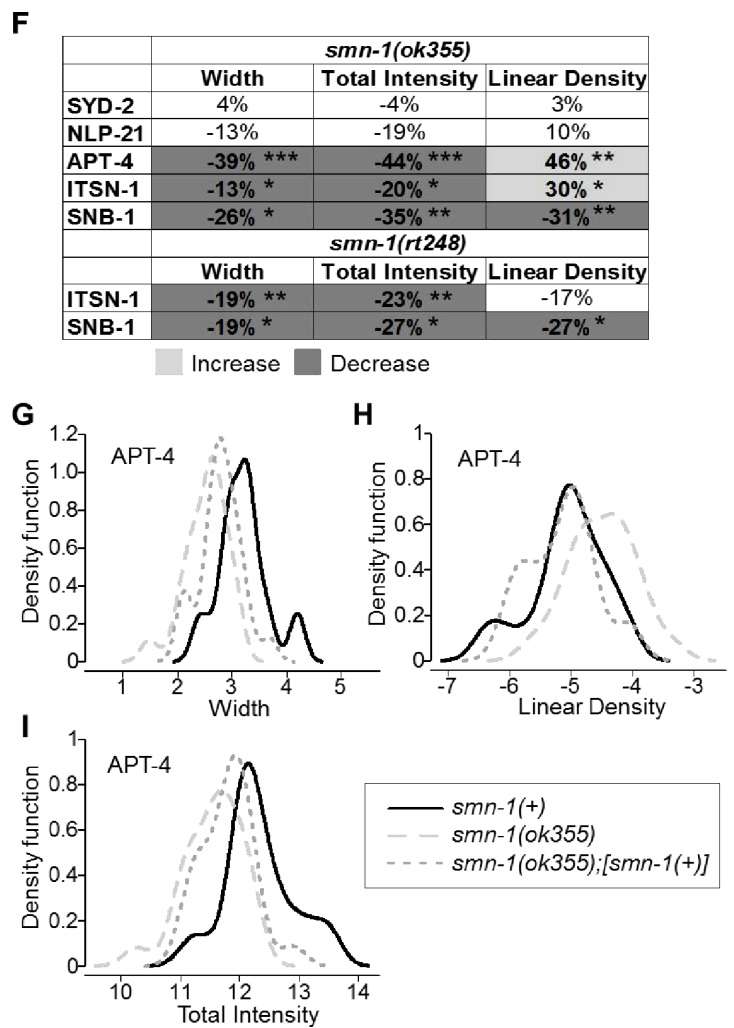
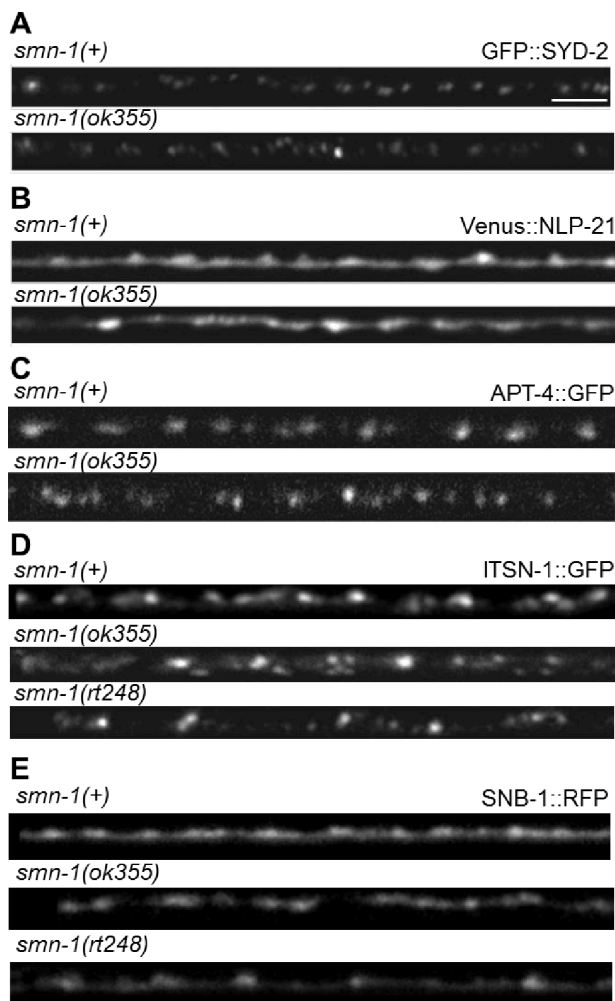


Fig. 3. Altered localization of presynaptic endocytic proteins in *smn-1* loss of function animals. (A-E) Representative images of fluorescently-tagged, presynaptic proteins expressed in the dorsal nerve cord of cholinergic DA motor neurons of *smn-1(+)* control, *smn-1(ok355)*, and *smn-1(rt248)* animals. Scale bar, 10 μ m. (F) Percent change from control for SYD-2 (α -liprin), NLP-21 (GGARAF neuropeptide family), APT-4 (AP2 α -adaptin), ITSN-1 (DAP160/Intersectin) and SNB-1 (synaptobrevin) in *smn-1(ok355)* animals is reported for average puncta width, puncta total intensity, and linear density (number/ μ m). ITSN-1 and SNB-1 are reported for *smn-1(rt248)*. Light and dark shading indicates an increase or decrease, respectively, in the *smn-1(ok355)* and *smn-1(rt248)* animals compared to *smn-1(+)* control (See Dataset S1 for extended analysis). Mann-Whitney *U*-test, two tailed * $p < 0.05$, ** $p < 0.01$, *** $p < 0.001$. (G-I) A single copy of the [*smn-1(+)*] construct *rtSi10* fully rescued APT-4 linear density (Control *smn-1(+)* animals versus rescued *smn-1(ok355);rtSi10[smn-1(+)]*) $p = 0.5$; *smn-1(ok355)* versus rescued $p = 0.002$, partially ameliorated puncta width defects (control *smn-1(+)* versus rescued $p = 0.002$; *smn-1(ok355)* versus rescued $p = 0.03$), but may not have improved total intensity (control *smn-1(+)* versus rescued $p = 5e-04$; *smn-1(ok355)* versus rescued $p = 0.09$). Distributions of APT-4 puncta width, linear density, and puncta total intensity in *smn-1(ok355)* animals is compared to distributions in control *smn-1(+)* and rescued animals. Results are presented as kernel density estimates, which convert distribution histograms into smooth, continuous density function curves. X-axis values were log₂-transformed prior to the calculation of the density function. Linear density (puncta/ μ m) values are less than 1 resulting in negative values after log₂ transform (Dataset S1). At least three independent trials performed ($n > 25$ animals in total/genotype).

I(ok355) and *smn-1(rt248)* were hypersensitive in their response to levamisole ($p = 0.02$ *smn-1(ok355)* and $p = 5e-4$ *smn-1(rt248)* vs *smn-1(+)*, Figure 1E). According to Miler and colleagues (42) a normal or hypersensitive response to levamisole suggests that an impaired ACh response at the muscle is not the cause of aldicarb resistance. Together, these data suggest that SMN-1 likely impacts presynaptic function and is required for normal neurotransmitter release.

Genetic interaction of *smn-1* with endocytic pathway genes.

The *smn-1(ok355)* and *smn-1(rt248)* synaptic defects could be due to impairments in the synaptic vesicle (SV) cycle. Potential functional interactions between *smn-1* and genes encoding SV endo- or exocytosis proteins were examined by constructing double mutant strains. For this epistasis analysis, we used two quantitative neuromuscular phenotypes: aldicarb sensitivity and

pharyngeal pumping rates. First, double mutant animals were constructed with *smn-1(ok355)* and complete (null) loss of function alleles for *unc-57* (endophilin-A) and *unc-26* (synaptojanin), which encode proteins in the synaptic clathrin-mediated endocytosis (CME) pathway (43), and *sdpn-1* (syndapin), which is required for activity-dependent bulk endocytosis (ADBE) (44). Loss of *smn-1* did not exacerbate the aldicarb resistance defects of *unc-57(ok310)* nor *unc-26(s1710)* compared to each single mutant strain, but rather an intermediate defect was observed (Figure S4A and S4B). The aldicarb response of *smn-1(ok355-);sdpn-1(ok1667)* animals was almost identical to that of *smn-1(ok355)* animals ($p = 0.76$, Figure S4C). When double mutant strains were constructed with complete (null) loss of function mutants involved in SV exocytosis, *snb-1* (synaptobrevin) or *unc-18* (Munc18), the aldicarb response defects were non-additive (p

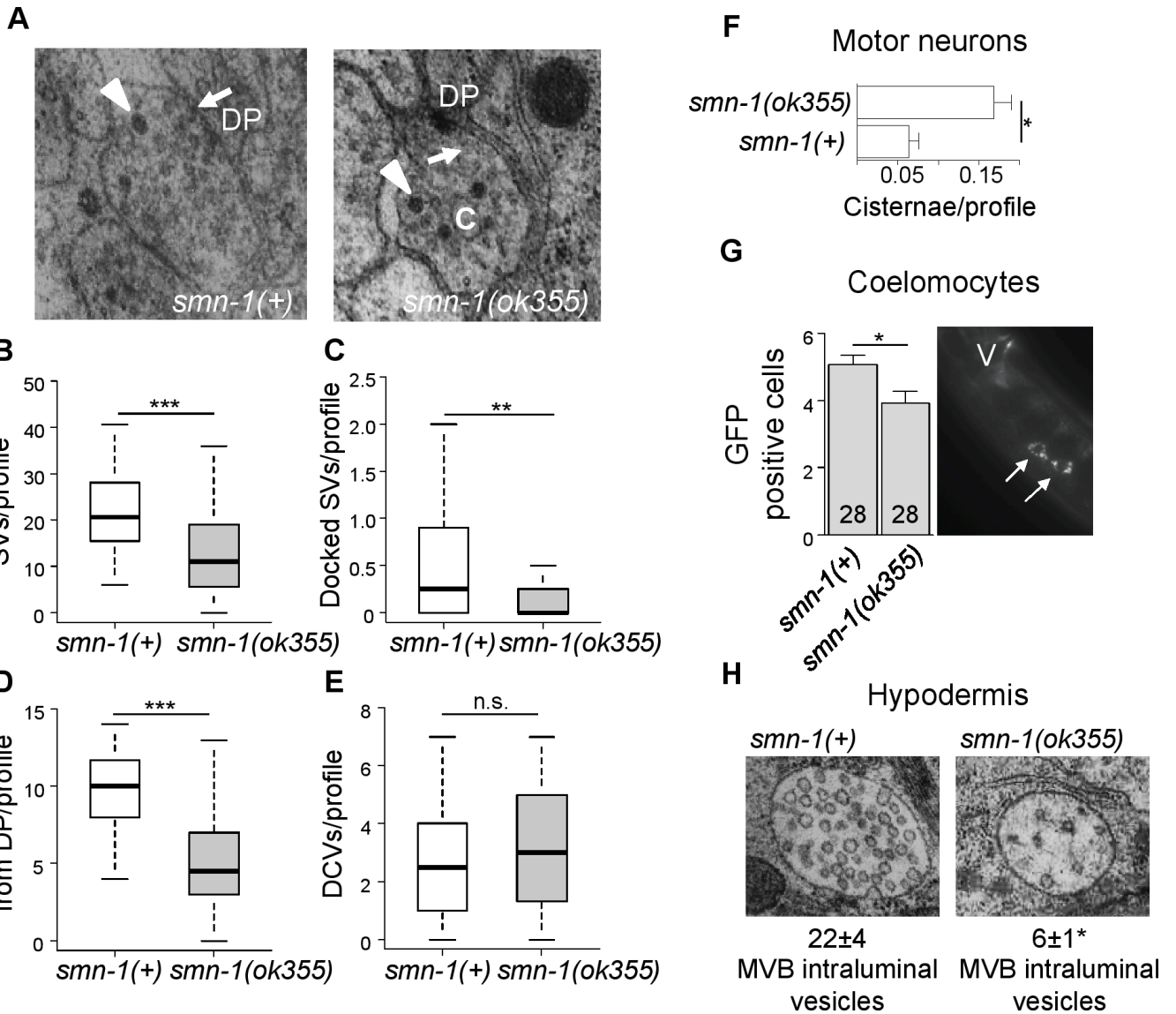


Fig. 4. Endosomal defects are seen in *smn-1(ok355)* motor neurons and elsewhere. (A) Representative electron micrograph images of *smn-1(+)* control and *smn-1(ok355)* neuromuscular junctions. Arrows point to synaptic vesicles (SVs) and arrowheads to dense core vesicles (DCVs). DP indicates dense projection; C indicates a cisterna. (B) SVs per synaptic profile, as defined by the presence of a DP, were reduced in *smn-1(ok355)* animals. Mann-Whitney *U*-test, two tailed: $***p < 0.001$. (C) Docked SVs in contact with the DP were reduced in *smn-1(ok355)* animals. Mann-Whitney *U*-test, two tailed: $**p < 0.01$. (D) *smn-1(ok355)* animals had reduced numbers of SVs within the region 100 nm from the synaptic profile/DP. Mann-Whitney *U*-test, two tailed: $***p < 0.001$ (Table S2). (E) The number of DCVs per synaptic profile/DP in *smn-1(ok355)* animals was not different than control *smn-1(+)* animals. Mann-Whitney *U*-test, two tailed: n.s., not significant. (F) Cisternae accumulated aberrantly in motor neurons of *smn-1(ok355)* mutants. Mean \pm SEM is shown, Mann-Whitney *U*-test, two tailed: $*p < 0.05$. (G) Fluid-phase endocytosis by coelomocytes was decreased in *smn-1(ok355)* animals, Mann-Whitney *U*-test, two tailed: $*p < 0.05$. Image on the right shows the pair of coelomocyte cells lying just anterior to vulva; arrows indicate GFP accumulation inside the coelomocytes. No GFP accumulation in the body cavity of *ok355* animals was observed. (H) Representative electron micrograph images of multivesicular bodies (MVBs) in the hypodermis of *smn-1(+)* control and *smn-1(ok355)* animals. The MVBs of *smn-1(ok355)* animals contained fewer intraluminal vesicles compared to *smn-1(+)* control animals, Mann-Whitney *U*-test, two tailed: $*p < 0.05$.

= 0.55 for *snb-1(md247)* vs *smn-1(ok355);snb-1(md247)* and $p = 0.72$ for *unc-18(e234)* vs *smn-1(ok355);unc-18(e234)*, Figures S4D and S4E). These results are consistent with *smn-1* depletion impairing SV function, but definitive conclusions could not be drawn. Therefore, we turned to pharyngeal pumping rates to assess genetic interactions (Figure 2A). Loss of *C. elegans* endophilin, synaptojanin or syndapin did not exacerbate the decreased pharyngeal pumping rates of *smn-1(ok355)* ($p = 0.34$ for *smn-1(ok355) unc-57(ok310)*, $p = 0.93$ for *smn-1(ok355);unc-26(s1710)* and $p = 0.67$ for *smn-1(ok355);sdpn-1(ok1667)*, Figures 2B, 2C and 2D). By contrast, double mutant strains with genes involved in SV exocytosis were additive and had significantly

reduced pumping rates compared to each single mutant strain ($p = 0.01$ for *smn-1(ok355);unc-18(e234)* and $p = 0.008$ for *smn-1(ok355);snb-1(md247)*, Figures 2E and 2F). Overall, these results indicate that SMN-1 depletion impairs synaptic transmission, potentially by decreasing SV recycling.

Diminished SMN-1 alters the presynaptic structure of motor neurons. If SV recycling is defective when SMN levels are diminished, then the localization and/or levels of specific presynaptic proteins might change. Synaptic localization was examined in the DA motor neurons of *smn-1(ok355)* and *smn-1(rt248)* animals for two fluorescently-tagged presynaptic proteins: SNB-1 (synapto-brevin) and ITSN-1 (DAP160/Intersectin) (45, 46). In the dorsal

681
682
683
684
685
686
687
688
689
690
691
692
693
694
695
696
697
698
699
700
701
702
703
704
705
706
707
708
709
710
711
712
713
714
715
716
717
718
719
720
721
722
723
724
725
726
727
728
729
730
731
732
733
734
735
736
737
738
739
740
741
742
743
744
745
746
747
748

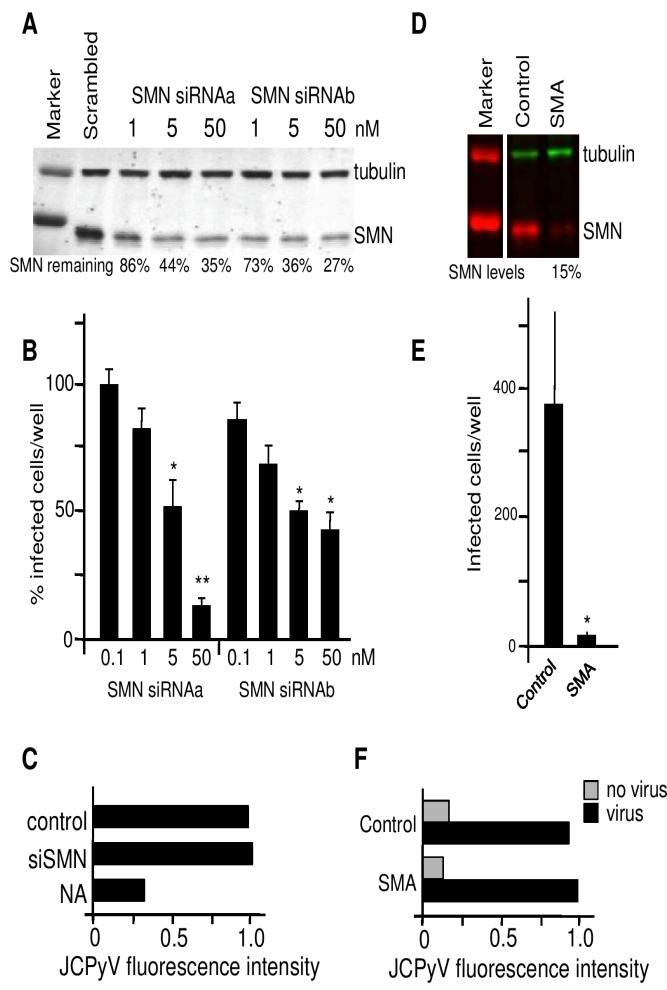


Fig. 5. Low SMN levels decrease JCPyV infection, but not virus binding. (A) SMN siRNA knockdown in SVG-A cells. SVG-A cells reverse-transfected with siRNAs specific for SMN; protein levels were determined by SDS-PAGE and immunoblot analysis using antibodies specific for SMN or tubulin (loading control). Percentage remaining SMN is indicated. (B) JCPyV infection is dependent on SMN. SVG-A cells were reverse-transfected with SMN siRNAs, infected with JCPyV and quantified based on nuclear VP1 staining. Here, we report the percentage of infected cells, relative to the siRNA scrambled control ($n=3$ independent experiments). For each experiment, 5 fields of view of a 12 well plate were scored for infection and each was compared to siRNA scrambled control (100%). Error bars indicate SEM; Student's t-test, two tailed: $*p < 0.05$, $**p < 0.01$. (C) JCPyV binding to SVG-A cells is not affected by SMN knockdown. Following siRNA-knockdown of SMN, SVG-A cells were either treated or untreated with neuraminidase (NA). Cells were incubated with JCPyV-633 and analyzed by flow cytometry. Data represent the relative fluorescence intensity of JCPyV-633 binding to cells normalized to control. (D) SMN protein levels in fibroblasts from an individual with SMA and control fibroblasts were determined by SDS-PAGE and immunoblot analysis using antibodies specific for SMN or tubulin (loading control). SMN levels are represented as % control SMN. (E) Fibroblasts derived from an SMA patient do not support JCPyV infection. Fibroblast cells were infected with JCPyV and quantified based on nuclear VP1 staining. Bar graphs represent the average number of infected cells/well for 3 wells and represent data from 3 independent experiments. Error bars indicate standard deviation (SD); Student's t-test, two tailed: $*p < 0.05$. (F) JCPyV binding is not decreased in SMA patient fibroblasts. SMA patient and control fibroblasts were incubated with JCPyV-633 and analyzed by flow cytometry. Relative fluorescence intensity of JCPyV-633 binding to cells normalized to control is indicated.

cord, DA motor neurons have no presynaptic inputs and form *en passant* synapses onto muscle processes (47). This results in a punctate pattern of protein localization along the length of the dorsal cord, composed primarily of presynaptic active zones (45).

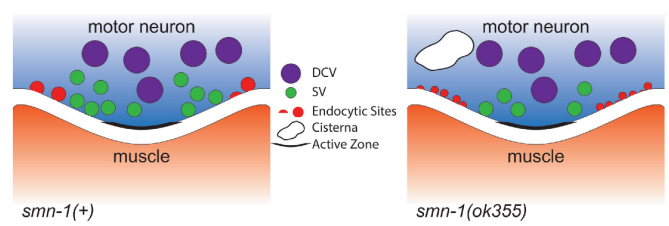


Fig. 6. The motor neurons of *smn-1(ok355)* animals display endocytic defects. Schematic summary of puncta and TEM analysis. The number of active zones and dense core vesicles (DCV) in *smn-1(ok355)* motor neurons was unchanged, but fewer presynaptic docked vesicles were observed, more irregular large vesicles, called cisternae, and aberrant localization of both AP2 α -adaptin and Intersectin/DAP160 endocytic proteins was observed in *smn-1(ok355)* motor neurons.

We quantified puncta width, puncta total intensity, and puncta linear density (number/ μm). In both *smn-1(ok355)* and *smn-1(rt248)* animals, puncta of the SV protein SNB-1 were diminished in width, intensity and density (average puncta width decreased 26% and 19% for *ok355* and *rt248*, respectively, $p = 0.02$ for *ok355* and $p = 0.04$ for *rt248*; average total intensity decreased 35% and 27% for *ok355* and *rt248*, respectively, $p = 0.005$ for *ok355* and $p = 0.02$ for *rt248*; density decreased roughly 30% for both alleles; $p = 0.004$ for *ok355* and $p = 0.01$ for *rt248*, Figure 3E and 3F). Puncta of the endocytic protein ITSN-1 (DAP160/Intersectin) were also altered in width and intensity in both *smn-1(ok355)* and *smn-1(rt248)* animals; linear density changed only in *smn-1(ok355)* animals (Figure 3D and 3F). ITSN-1 puncta were smaller in size (ITSN-1 average puncta width decreased by 13% and 19% for *ok355* and *rt248*, respectively, $p = 0.03$ for *ok355* and $p = 0.008$ for *rt248*). Puncta total ITSN-1 intensity was reduced by 20% and 23% for *ok355* and *rt248*, respectively, $p = 0.02$ for *ok355* and $p = 0.004$ for *rt248*.

As both *smn-1* loss of function alleles had the same profile, we also examined three more presynaptic markers in the cholinergic DA motor neurons of *smn-1(ok355)* animals only: SYD-2 (α -liprin), NLP-21 (GGARAF neuropeptide family) and APT-4 (AP2 α -adaptin). SYD-2 and NLP-21 puncta were unaltered in *smn-1(ok355)* animals, suggesting that the number of synapses - based on active zones and dense core vesicles (DCV), respectively - is unchanged when SMN-1 levels drop (Figure 3A, 3B and 3F). This is consistent with previous work showing that *smn-1(ok355)* animals have no overt defects in nervous system morphology and no motor neuron death (31). Puncta of the endocytic APT-4 (AP2 α -adaptin) were altered in intensity and number in *smn-1(ok355)* animals (Figure 3C and 3F). APT-4 puncta were more numerous along the neuronal processes (APT-4 increased 46%, $p = 0.003$), but were smaller in size (APT-4: decreased 39%, $p = 8e-06$). Puncta total intensity was reduced by 44% for APT-4 ($p = 3e-05$). To further confirm that changes in synaptic protein levels were due to decreased *smn-1* function, a wild type copy of *smn-1(+)* was introduced to *smn-1(ok355)* animals expressing APT-4::GFP. Synaptic defects were ameliorated or eliminated (Figure 3G, 3H and 3I). Combined, these results suggest that *smn-1* loss of function likely causes defects in SV recycling resulting in aberrant localization of endocytic proteins and fewer functional synaptic vesicles. To confirm this interpretation, we examined *smn-1(ok355)* presynaptic specializations at a higher resolution.

Decreased *smn-1* function causes defects in endocytic compartments. We sectioned and reconstructed part of the ventral nerve cord for both normal *smn-1(+)* and mutant *smn-1(ok355)* animals to determine the number and distribution of vesicles in the presynaptic specializations by using transmission electron microscopy (TEM) (Figure 4A). The total number of SVs per presynaptic region was reduced by 36% in motor neurons of *smn-1(ok355)* animals versus *smn-1(+)* (14 ± 2 , $n=45$ versus 22 ± 2 , 810

749
750
751
752
753
754
755
756
757
758
759
760
761
762
763
764
765
766
767
768
769
770
771
772
773
774
775
776
777
778
779
780
781
782
783
784
785
786
787
788
789
790
791
792
793
794
795
796
797
798
799
800
801
802
803
804
805
806
807
808
809
810
811
812
813
814
815
816

n=35, respectively, $p = 0.0002$, Figure 4B). The average number of docked vesicles at the plasma membrane ($p = 0.008$) and average number of SVs 100 nm away from the active zone ($p = 4e-08$) were also decreased in *smn-1(ok355)* animals versus *smn-1(+)* (Figure 4C and 4D). By contrast, the average number of DCVs in each presynaptic profile was not significantly different between *smn-1(+)* and *smn-1(ok355)* animals ($p = 0.34$, Figure 4E). The changes observed in synaptic vesicles were consistent with results from the puncta analysis (Figure 3). TEM studies also revealed an unusual accumulation of cisternae in *smn-1(ok355)* synapses (Figure 4F). Cisternae are large and abnormal-sized vesicles that often reflect arrested endocytic vesicle maturation and sorting. Cisternae accumulation was reported in the synapses of *C. elegans* defective in endocytosis, such as *unc-57* and *unc-26* animals (43, 48). *smn-1(+)* animals had 0.06 ± 0.01 cisternae/synaptic specialization, whereas *smn-1(ok355)* animals exhibited a three fold increase (0.17 ± 0.02 cisternae/profile; $p = 0.02$). The ultrastructural abnormalities in *smn-1(ok355)* animals further support a model in which diminished SMN-1 function impairs endosomal trafficking in motor neuron synapses.

Diminished SMN-1 causes endosomal defects in non-neuronal tissues. Synaptic vesicle recycling shares common elements with endosomal trafficking in other cells. To determine if *smn-1* depletion causes endosomal defects more broadly, other tissues were examined. The *C. elegans* body cavity contains six coelomocyte cells that rely on fluid-phase endocytosis to clear soluble moieties from the pseudocoelom (49). Animals engineered to secrete GFP from body wall muscles into the body cavity have been used extensively to characterize endocytic activity in coelomocyte cells (50). We compared coelomocyte GFP uptake in *smn-1(+)* and *smn-1(ok355)* animals. GFP uptake in *smn-1(ok355)* animals (Figure 4G, $p = 0.01$) is significantly reduced, indicating that diminished SMN-1 causes endocytic pathway defects in these non-neuronal cells. As GFP does not accumulate in the body cavity of *smn-1(ok355)* animals, the coelomocytes defect is not severe. To confirm that *smn-1* loss decreases endocytosis, we used RNAi to knock down SMN-1 specifically in coelomocytes. Loss of SMN-1 resulted in increased GFP intensity in coelomocytes and significant accumulation of GFP in the body cavity, consistent with stalled endocytosis and a cell-autonomous defect. No gross morphology changes or large vacuoles were observed (Figures S5 and S6).

Next, the impact of SMN depletion on late endosomal/lysosomal compartments was examined by assessing multivesicular body (MVB) morphology in TEM sections. MVBs contain internal intraluminal vesicles that can be degraded in the lysosome or transported to the cellular membrane for recycling/secretion. In *smn-1(ok355)* animals, the average number of MVB intraluminal vesicles per MVB was dramatically decreased compared to *smn-1(+)* animals (22 ± 4 versus 6 ± 1 , $p = 0.002$, Figure 4H) suggesting that diminished SMN-1 impacts either generation or clearance of intraluminal vesicles in this late endosomal compartment. The average diameter of MVBs in *smn-1(ok355)* animals was unaffected in relation to controls ($p = 0.81$). Additionally, apical (luminal) endocytosis in the intestine of *smn-1(ok355)* animals was tested by feeding nematodes rhodamine-dextran. No difference in the endocytosis-dependent accumulation of fluorescence in intestinal cells was observed in *smn-1(ok355)* versus *smn-1(+)* animals (Figure S7). Overall, these results demonstrate that SMN-1 depletion causes endocytic pathway defects in motor neurons and in other tissues.

Decreased SMN impairs endocytosis-dependent viral infection. Endocytic trafficking is required for multiple cellular events in both invertebrates and vertebrates, including infection by pathogenic organisms. Many viruses use cellular endocytic pathways to enter cells and reduction of classical endocytic proteins impairs viral infection in *Drosophila* (51) and human cells (52-54).

To determine whether the defects caused by diminished SMN in *C. elegans* are conserved in vertebrates, we examined endocytosis-dependent infection of human cells by a virus known to use the endocytic pathway for entry and internalization. JCPyV binds to cell surface receptors and enters cells via clathrin-mediated endocytosis (52-54). Initially, we tested two different siRNAs and found that both depleted SMN in SVG-A glial cells that support JCPyV infection (Figure 5A). To determine whether JCPyV infection was reduced by *SMN1* knockdown, we compared infection in SMN-depleted cells versus control scrambled siRNA-treated cells; decreased SMN impaired JCPyV infection (Figure 5B). To rule out an effect on virus binding prior to endocytosis, we assessed the binding of fluorescently-labeled virus (JCPyV-633) to glial cells treated with SMN-specific or control siRNA by flow cytometry. Binding of JCPyV-633 to glial cells was not affected when SMN levels were decreased by siRNA treatment (Figure 5C). However, binding was reduced when cells were pre-treated with neuraminidase, indicating that JCPyV bound to the appropriate sialic acid receptor (Figure 5C) (55, 56). To confirm the impact of SMN knockdown on infection, the same experiments were undertaken using commercially available fibroblasts from an unaffected carrier and a Type I SMA patient. SMA Type I fibroblasts were resistant to infection, while virus binding was equivalent to control fibroblasts from a carrier individual with normal SMN levels (Figures 5D-5F). Collectively, these data suggest that decreased SMN levels result in resistance to JCPyV infection. Overall, SMN depletion may impair infection at the stage of endosomal trafficking and/or at subsequent steps in the infection cycle.

Discussion

Despite decades of work we still do not know why decreased SMN levels causes abnormal synaptic organization and defective synaptic neurotransmission in SMA. Here, we report for the first time that decreased SMN protein levels impair endocytic pathways, which have not been previously implicated in SMA pathogenesis. The majority of the work presented here is based on a previously defined *C. elegans* model of SMA in which decreased function of the *C. elegans* SMN ortholog, SMN-1, results in neuromuscular functional defects, without motor neuron death. We found that the motor neurons of *smn-1* loss of function animals had reduced numbers of presynaptic docked vesicles, inappropriately high numbers of irregular vesicles called cisternae, aberrant localization of endocytic proteins, and decreased synaptobrevin levels. Additionally, genetic interactions of *smn-1* with known components of the synaptic vesicle cycle suggested that endocytosis was impaired. Combined, these results indicate impaired synaptic vesicle recycling and perturbed endocytic pathway function (Figure 6). We also observed defects in the endosomal compartments of non-neuronal tissues, consistent with the observation that SMA has consequences outside the neuromuscular system. Finally, SMN depletion reduced endocytosis-dependent viral infection in human cells, but did not affect virus binding, consistent with results from the *C. elegans* SMA model. Combined these results suggest that impaired endocytic trafficking may be a major player in SMA pathology.

Depletion of SMN has widespread endocytic consequences. Neuromuscular defects are the most obvious hallmarks of SMA, but SMN is ubiquitously expressed and numerous studies have suggested non-neuronal requirements for SMN function in heart (57-59), liver (60), muscle vascular system (61), lung, intestine (62), and in pancreatic islets (63). Therefore, it was not surprising that endosomal defects were observed in other *C. elegans* tissues when SMN levels were compromised. SMN-1 reduction led to impaired endocytic trafficking by coelomocyte cells, which clear the body cavity of small solutes. Also, the number of intraluminal vesicles in hypodermal late endosomes/MVBs was decreased by

72% in *smn-1* mutants, suggesting that defects in transmembrane receptor recycling/clearance may occur when SMN levels are diminished. Endosomal pathways play critical roles in protein trafficking and receptor signaling in all tissues. Overall, our results suggest that endosomal defects may contribute to the systemic problems of SMA patients.

SMN-depleted cells are resistant to viral endocytosis-dependent infection. To independently assess the impact of SMN depletion on endocytic pathways, we turned to an established model of endocytosis-dependent viral infection. In *Drosophila*, heterozygous mutations in genes involved in endocytosis result in resistance to *Drosophila* C virus infection, consistent with a critical role for endocytosis in infection and pathogenesis (51). Here, we report that SMN depletion results in decreased JCPyV infection both in cells treated with SMN siRNA and in SMA patient-derived cells. There are multiple steps in viral endosomal trafficking and infection that may be impacted by diminished SMN but viral attachment was not affected. The results presented here are consistent with SMN decrements affecting viral infection that is dependent on endocytosis, but viral infection is complex and further studies will be required to determine how diminished SMN decreases infection. A link between decreased SMN levels and increased resistance to viral endocytosis-dependent infection would be of significant interest and might explain why SMA mutant alleles are common. To our knowledge, a link between SMN levels and infection has not been examined previously. The SMA heterozygosity frequency (1:40 to 1:60) is similar to the frequency observed for sickle cell anemia and cystic fibrosis alleles, which are known to confer carrier survival benefits in populations at risk. (64-66). SMA alleles frequently arise *de novo* via chromosome rearrangement and in some cases the neighboring neuronal apoptosis inhibitory protein (*NAIP*) gene is deleted (4). Mice lacking the *NAIP* gene fail to activate a response to *Legionella pneumophila* infection (67), but results herein suggest a role for SMN should be considered in future studies.

How could SMN regulate endocytic trafficking? Two nonexclusive models may explain why diminished SMN causes endocytic pathway defects. In the first model, SMN depletion leads to aberrant trafficking or splicing of mRNAs that encode proteins critical for endocytic function. For example, SMN loss impairs axonal transport of RNP granules containing mRNAs that encode numerous proteins, including: annexin 2, annexin 3 and Rab18 (68); their loss may result in endosomal defects. Or more indirectly, loss of SMN may cause missplicing of mRNAs that encode proteins with a role in endocytic trafficking; mRNAs such as annexin 2 are known to be misspliced when SMN levels are depleted (69). In the second model, SMN is part of an RNA/protein complex that promotes endocytic trafficking. SMN directly binds and is transported within axons with the alpha subunit of the coat protein 1 (COPI), a critical player in intracellular vesicular trafficking. COPI can be found on Golgi, ER and MVB membranes and COPI loss results in defective endosomal function (70-72). Alternatively, the functional interaction between SMN, Plastin 3 and actin might play a role in the endocytic pathway defects observed when SMN levels are depleted. Plastin 3, an actin-bundling protein was identified as a gender-protective SMA modifier and was found in a protein complex along with SMN and actin (73). Loss of fimbrin, the yeast PLS3 ortholog, inhibits endocytosis (74) and Plastin 3 interacts with activated Rab5 to facilitate mammalian endocytosis (75). Also, actin filaments can form a critical collar-like structure around the neck of endocytic vesicles as they pull away from the cell membrane (76-78), but it is unclear if SMN or Plastin 3 are associated with these structures. Hence, we consider it possible that SMN and Plastin 3 are essential players of a protein complex required for endocytic trafficking, but additional studies will be needed to determine

which of these models best explains the endosomal defects caused by SMN reduction.

Conclusions. The genetic, pharmacological and functional studies presented here demonstrate that SMN depletion impacts endocytic trafficking. Previous studies connect endocytosis and endosomal trafficking with other neurodegenerative diseases. For example, over-expression of the endosomal protein Rab11 reverses the synaptic transmission and vesicular deficits caused by mutant huntingtin in a *Drosophila* model of Huntington's disease (HD) (79). Furthermore, *CHMP2B* mutations cause frontotemporal dementia (FTD) and impair endosome-lysosome fusion (80). Additionally, Farg and co-workers identified a role in Rab-mediated endosomal trafficking for C9ORF72, a cause of sporadic Amyotrophic Lateral Sclerosis (ALS) (81). Finally, *BICD2* mutations are linked to autosomal-dominant SMA (82), and notably loss of the *BICD2* *Drosophila* ortholog impairs clathrin-mediated endocytosis at presynaptic specializations (83). Identifying the functionally relevant components that connect diminished SMN levels to endocytic pathways could lead to the identification of novel therapeutic interventions for SMA and related neurodegenerative disorders.

Materials and Methods

C. elegans strains, constructs and transgenes. Strains listed in Table S1 were maintained at 20°C under standard conditions (84). For all experiments involving *smn-1(ok355)* or *smn-1(rt248)*, animals tested were first generation progeny of parents heterozygous for the *hT2* balancer. To maintain a common genetic background, control *smn-1(+)* animals were similarly derived from *+hT2* parents. Plasmid pHA#582 contains a 1819 bp fragment corresponding to the *smn-1* promoter, coding sequence and 3' untranslated region subcloned as an *AflIII/XhoI* product into pCFJ356 (Addgene plasmid 34871) (85). Primers for amplification: 5-tgatcttaagtctacgagcgacattcatcg and 5-tgatctcgagcagcctctctctgattgc. *rtSi9[Cb-unc-119(+)]IV* and *rtSi10[smn-1p::smn-1;Cb-unc-119(+)]IV* transgenes were generated by *Mos1*-mediated single-copy insertion (85, 86). 50 ng/μl of targeting plasmid (pCFJ356 or pHA#582) was injected into EG6703 (*unc-119(ed3)III;cxT10816 IV*) animals along with 50 ng/μl pCFJ601 (*eft-3p::Mos1* transposase), 10 ng/μl pGH8 (*rab-3p::mCherry*), 5 ng/μl pCFJ104 (*myo-3p::mCherry*) and 2.5 ng/μl pCFJ90 (*myo-2p::mCherry*). Insertion events were identified based on rescue of *unc-119* in non-fluorescent animals and confirmed by PCR-genotyping, prior to crossing into *smn-1(ok355)/hT2*. In Figures 1A, B and D and in Figure 3 G, H and I, *smn-1(ok355);[smn-1(+)]* animals carry *rtSi10*. For these same figures, *smn-1(+)* and/or *smn-1(ok355)* animals carry *rtSi9*, which differs from *rtSi10* only in the absence of an *smn-1(+)* gene copy. The small guide RNA (sgRNA) plasmid targeting the *smn-1* gene (pHA#730) for CRISPR/Cas9-mediated genome editing was generated by amplification of *Pu6::klp-12* (35) and subsequent ligation of the PCR product obtained by primers: 5'- AACATCGTCAAACATTAGAT-TTGCAATTCAATTATATAGGGACC-3' and 5'- TGGGATGATAGTTTTAGAGCTA-GAAATAGCAAGTTAAAATAAGGC-3'. The resulting plasmid was injected at 50 ng/μl into wild type animals following the *dpy-10(cn64)* co-conversion protocol from Arriberre *et al.*, 2014 (34). After backcross, the resulting *smn-1(rt248)* allele was balanced over the *hT2* chromosomal translocation. *smn-1(rt248)* creates D19fs and likely eliminates SMN-1 function.

C. elegans behavioral assays. Pharyngeal pumping assays were performed in the last larval stage as previously described (32). Grinder movement in any axis was scored as a pumping event. Average pumping rates (\pm SEM) were combined from at least three independent trials ($n > 25$ animals in total/genotype). Aldicarb and levamisole assays on early L4 stage larval animals were carried out blinded as to genotype in at least three independent trials ($n \geq 30$ animals in total/genotype) as described elsewhere (38, 87). Drug-induced paralysis caused by 1 mM aldicarb (Sigma) or 0.4 mM levamisole (Sigma) was scored as inability to move/pump in response to prodding with a metal wire.

C. elegans light level microscopy. Early L4 stage larval animals were mounted on 2% agar pads and immobilized using 30 mg/ml BDM (Sigma) in M9 buffer. Images were captured as Z-stacks from the dorsal cord above the posterior gonad reflex (100x objective, Zeiss AxioImager ApoTome and AxioVision software v4.8). At least three independent trials ($n > 25$ animals in total/genotype) were undertaken. Puncta total intensity, width and linear density were quantified using the 'Punctaanalyser' program in Matlab (88). Kernel density estimation of the puncta population was determined in R (v3.0.3). Invariant fluorescent illumination was confirmed daily using 0.5 μm fluorescent beads (FluoSpheres, Molecular Probes) (46). Coelomocyte imaging was undertaken blinded as to genotype in three independent trials ($n > 25$ animals in total/genotype). GFP levels in the six coelomocytes of early L4 stage animals were assessed using a Zeiss V20 stereoscope (50).

C. elegans transmission electron microscopy. Animals were prepared in parallel for transmission electron microscopy as described (89). Briefly, early L4 nematodes were fixed by a high-pressure freezing apparatus followed

1089 by a 2% osmium in acetone freeze substitution. Ultra-thin serial sections
1090 (50-60nm thickness) were collected on Formvar/Pioloform-coated copper
1091 slot grids, stained with 4% uranyl acetate in 70% methanol, followed by
1092 washing and lead citrate incubation. Images were obtained on a Philips CM10
1093 transmission electron microscope using an Olympus Morada camera system
1094 driven by the iTEM software (Olympus Soft Imaging Solutions). Image registra-
1095 tion and annotation was performed using TrakEM2 (90). Three hundred
1096 and five hundred serial sections were imaged for control and *smn-1(ok355)*
1097 animals, respectively. The anterior ventral nerve cord was reconstructed from
1098 one animal for each genotype. Synapses were examined from VA and VB
1099 cholinergic neurons and the VD γ -aminobutyric acid (GABA) neuron (47).
1100 Thirty five control (27 cholinergic and 8 GABAergic) and 45 *smn-1(ok355)* (25
1101 ACh and 20 GABAergic) neuromuscular synapses were examined. The ratio of
1102 GABAergic to cholinergic (ACh) synapses was not significantly different from
1103 control, suggesting that ACh synapses are not preferentially lost (Chi-squared
1104 test, $p > 0.05$). A synapse was defined as a set of serial sections containing
1105 a dense projection. Docked vesicles were defined as those contacting the
1106 plasma membrane adjacent to a dense projection. The number of synaptic
1107 vesicles (~30 nm diameter) and dense core vesicles (~40 nm diameter) were
1108 counted in sections containing a dense projection and the numbers of each
1109 profile were averaged to obtain the final value. The presence of large clear
1110 vesicles/cisternae (>40 nm diameter) was analyzed by counting every other
1111 serial section within one micron to either side of a dense projection. For
1112 multivesicular bodies, the intraluminal vesicles were counted for >30 cell
1113 profiles per genotype.

1114 **Cells and viruses.** Cells were grown at 37°C in a humidified incubator
1115 with 5% CO₂. SVG-A cells are a subclone of the human glial cell line SVG
1116 transformed with an origin-defective SV40 mutant and grown in minimum
1117 essential medium (MEM) supplemented with 10% fetal bovine serum (FBS)
1118 and 1% penicillin-streptomycin (P/S) (Mediatech, Inc.) (91). Untransformed
1119 primary fibroblasts were from a patient with SMA Type I (GM09677) and
1120 control cells from a disease-free SMA carrier (GM03814) (Coriell Cell Reposi-
1121 tories). Fibroblasts were grown in MEM supplemented with 10% FBS and
1122 non-essential amino acids. Generation and propagation of the virus strain
1123 Mad-1/SVEΔ was previously described (92).

1124 **Transfection.** Cells were reverse-transfected with SMN-specific siRNAs
1125 using Lipofectamine RNAiMax (Life Technologies). SMN siRNAs (SMN siRNAa
1126 [Hs.SMN1_11]: ACGGTTGCATTTACCCAGCTA (Cat. No. SI04950932) and SMN
1127 siRNAb [Hs.SMN1_12]: ATCAGATAACATCAAGCCCAA (Cat. No. SI04950939))
1128 from Qiagen were prepared according to manufacturer's instructions. Serum-
1129 free medium was added to triplicate wells of a 12 well plate and siRNAs were
1130 diluted to a final concentration of 0.1, 1, 5, and 50 nM. Two microliter of
1131 RNAiMax Lipofectamine was added, solutions were mixed and incubated at
1132 room temperature (RT) for 20 min. Following incubation, 2 x 10⁵ cells in
1133 1 mL of media containing FBS was added to each well. Cells were incubated
1134 at 37°C for 36 h and then infected or harvested for protein quantitation by
1135 immunoblot analysis. Infection data were compared to cells transfected with
1136 Allstars siRNA negative control (Qiagen).

1137 **Infection.** Patient fibroblasts were plated to 60% confluency in 12
1138 well plates O/N. Cells from siRNA transfections were infected at 36 h post-
1139 transfection. Media was aspirated and cells were infected with a multiplicity
1140 of infection (MOI) of 5 (JCPyV) fluorescent focus units (FFU)/cell in MEM
1141 containing 2% FBS at 37°C for 1.5 h. Infected cells were then fed with
1142 2 mL of appropriate media and incubated at 37°C for 72 h. Cells were
1143 washed in 1X phosphate-buffered saline (PBS), fixed in cold methanol, and
1144 incubated at -20°C. Fixed cells were washed in PBS, permeabilized with 0.5%

1150 Triton X-100 (USB Corporation) at RT for 5 min, incubated with PAB597, a
1151 hybridoma supernatant that produces a monoclonal antibody against JCPyV
1152 VP1 (generously provided by Ed Harlow) (93), at a 1:10 dilution in PBS at 37°C
1153 for 1 h, washed with PBS, incubated with a goat anti-mouse Alexa Fluor 488-
1154 conjugated antibody (1:1000; 20 μ g/mL) (Life Technologies) in PBS at 37°C
1155 for 1 h, and washed again in PBS. Cells were analyzed for VP1 staining in the
1156 nucleus under a 20X objective using an Eclipse TE2000-U microscope (Nikon).

1157 **Immunoblot.** Cell lysates were prepared by washing cells in 200 μ L PBS,
1158 scraping, and collecting the lysates. Cells were centrifuged at 3000 rpm for
1159 5 min and pellets were resuspended in 1X RIPA buffer with protease (1:10)
1160 and phosphatase (1:100) inhibitors (Sigma) and incubated on ice for 30 min.
1161 Cells were pelleted at 14,000 rpm and supernatants were diluted at a 1:1
1162 ratio in SDS loading buffer, boiled at 95°C for 5 min, and 15 μ L was resolved
1163 by SDS-PAGE using a 4-15% Tris-HCL gel (BioRad). Gels were transferred to
1164 PVDF membranes (BioRad) using a Transblot system (BioRad) at 10V for 30
1165 min. Membranes were blocked in 2% milk in PBS with 0.1% Tween 20% (PBS-
1166 T) O/N, then incubated with a purified mouse anti-SMN primary antibody at
1167 1:5000 dilution (BD Biosciences; 610647) and an anti-alpha tubulin polyclonal
1168 antibody loading control at 1:450 dilution (Abcam; ab4074) at RT for 1 h,
1169 washed in PBS-T, then incubated with a 680 nM goat-anti-mouse secondary
1170 antibody at 1:1000 dilution (Life Technologies) and a 800 nM anti-rabbit
1171 secondary antibody at 1:5000 dilution (LI-COR Biosciences) at RT for 1 h.
1172 All antibodies were diluted in 2% milk. Immunoblots were scanned and
1173 analyzed using an Odyssey CLx Infrared Imaging System (LI-COR Biosciences).

1174 **Flow Cytometry.** All cells (SVG-A treated with SMN or control siRNAs or
1175 fibroblasts) (1 x 10⁶) were washed with PBS, incubated with cell stripper (Cell-
1176 gro), and removed from plates. Cells were pelleted, washed, and incubated
1177 in 100 μ L of PBS with 2.5 μ g of JCPyV labeled with Alexa Fluor 633 (JCPyV-
1178 633) or PBS alone for 2 h on ice. For neuraminidase treatment, cells were first
1179 incubated for 45 min at 37°C in the presence of 5 U/mL Type V neuraminidase
1180 from *Clostridium perfringens* (Sigma) or PBS control. Cells were pelleted and
1181 washed with PBS twice, resuspended in 1x PBS and analyzed for virus binding
1182 using a BD FACSCalibur equipped with a 633 nm laser line (BD Bioscience).
1183 Data were analyzed using FlowJo software (Tree Star, Inc.).

1184 **Statistical analysis.** Two-tailed Mann-Whitney U or Log-rank test was
1185 used for *C. elegans* statistical analysis. For JCPyV infection, p values were
1186 determined using an unpaired Student's t-test (two-tailed distribution).

1187 **ACKNOWLEDGEMENTS.** We thank the Kaplan, Jorgensen, and Zhen labs
1188 for advice on *C. elegans* fluorescent imaging and quantitation as well as
1189 Dr. M. McKeown for helpful discussions. The *C. elegans* Gene Knockout
1190 Consortium (NIH/NHGRI) and the National BioResource Project provided *C.*
1191 *elegans* strains. Additional strains were provided by the CGC, funded by NIH
1192 Office of Research Infrastructure Programs (P40 OD010440). This work was
1193 supported by the SMA Foundation and NIH NINDS (NS066888) to A.C.H, NIH
1194 OD010943 to D.H.H, NIH NINDS F31NS089201 to P.J.O, and by an Institutional
1195 Development Award (IDeA) from the National Institute of General Medical
1196 Sciences of the National Institutes of Health to M.S.M. (P20GM103423).
1197 Research in the Atwood laboratory is funded by P01NS065719 (W.J.A.),
1198 R01NS043097 (W.J.A.), and a Ruth L. Kirschstein National Research Service
1199 Award F32NS064870 (M.S.M.) from the National Institute of Neurological
1200 Disorders and Stroke. Core facilities for the Atwood laboratory are sup-
1201 ported by P30GM103410 (W.J.A) from the National Institute of General Medi-
1202 cal Sciences. Core facilities for electron microscopy at the Hall laboratory
1203 are supported by NICHD (P30 HD171593) for the RFK-IDDRC at Albert Einstein
1204 College of Medicine..

- 1205 proteins. *Cell* 90(6):1013-1021.
- 1206 12. Pellizzoni L, Kataoka N, Charroux B, & Dreyfuss G (1998) A novel function for SMN, the
1207 spinal muscular atrophy disease gene product, in pre-mRNA splicing. *Cell* 95(5):615-624.
- 1208 13. Hua Y & Zhou J (2004) Survival motor neuron protein facilitates assembly of stress granules.
1209 *FEBS Lett* 572(1-3):69-74.
- 1210 14. Zou T, et al. (2011) SMN deficiency reduces cellular ability to form stress granules, sensitizing
1211 cells to stress. *Cell Mol Neurobiol* 31(4):541-550.
- 1212 15. Akten B, et al. (2011) Interaction of survival of motor neuron and HuD proteins with mRNA
1213 epg15 rescues motor neuron axonal deficits. *Proc Natl Acad Sci U S A* 108(25):10337-10342.
- 1214 16. Fallini C, Bassell GJ, & Rossoll W (2012) Spinal muscular atrophy: the role of SMN in axonal
1215 mRNA regulation. *Brain Res* 1462:81-92.
- 1216 17. Pagliardini S, et al. (2000) Subcellular localization and axonal transport of the survival motor
1217 neuron protein in the developing rat spinal cord. *Hum Mol Genet* 9(1):47-56.
- 1218 18. Rossoll W, et al. (2003) Smn, the spinal muscular atrophy-determining gene product, mod-
1219 ulates axon growth and localization of beta-actin mRNA in growth cones of motoneurons. *J*
1220 *Cell Biol* 163(4):801-812.
- 1221 19. Todd AG, et al. (2010) SMN, Gemin2 and Gemin3 associate with beta-actin mRNA in the
1222 cytoplasm of neuronal cells in vitro. *J Mol Biol* 401(5):681-689.
- 1223 20. Zhang H, et al. (2006) Multiprotein complexes of the survival of motor neuron protein SMN
1224 with Gemin3 traffic to neuronal processes and growth cones of motor neurons. *J Neurosci*
26(33):8622-8632.
21. Pellizzoni L, et al. (2001) A functional interaction between the survival motor neuron complex
and RNA polymerase II. *J Cell Biol* 152(1):75-85.
22. Ning K, et al. (2010) PTEN depletion rescues axonal growth defect and improves survival in
SMN-deficient motor neurons. *Hum Mol Genet* 19(16):3159-3168.

1225
1226
1227
1228
1229
1230
1231
1232
1233
1234
1235
1236
1237
1238
1239
1240
1241
1242
1243
1244
1245
1246
1247
1248
1249
1250
1251
1252
1253
1254
1255
1256
1257
1258
1259
1260
1261
1262
1263
1264
1265
1266
1267
1268
1269
1270
1271
1272
1273
1274
1275
1276
1277
1278
1279
1280
1281
1282
1283
1284
1285
1286
1287
1288
1289
1290
1291
1292

23. Sanchez G, et al. (2013) A novel function for the survival motoneuron protein as a translational regulator. *Hum Mol Genet* 22(4):668-684.

24. Grice SJ & Liu JL (2011) Survival motor neuron protein regulates stem cell division, proliferation, and differentiation in *Drosophila*. *PLoS Genet* 7(4):e1002030.

25. Kariya S, et al. (2008) Reduced SMN protein impairs maturation of the neuromuscular junctions in mouse models of spinal muscular atrophy. *Hum Mol Genet* 17(16):2552-2569.

26. Le TT, et al. (2005) SMNDelta7, the major product of the centromeric survival motor neuron (SMN2) gene, extends survival in mice with spinal muscular atrophy and associates with full-length SMN. *Hum Mol Genet* 14(6):845-857.

27. Lee YI, et al. (2011) Muscles in a mouse model of spinal muscular atrophy show profound defects in neuromuscular development even in the absence of failure in neuromuscular transmission or loss of motor neurons. *Dev Biol* 356(2):432-444.

28. Kong L, et al. (2009) Impaired synaptic vesicle release and immaturity of neuromuscular junctions in spinal muscular atrophy mice. *J Neurosci* 29(3):842-851.

29. Torres-Benito L, et al. (2011) SMN requirement for synaptic vesicle, active zone and microtubule postnatal organization in motor nerve terminals. *PLoS One* 6(10):e26164.

30. Martinez-Hernandez R, et al. (2013) Synaptic defects in type I spinal muscular atrophy in human development. *J Pathol* 229(1):49-61.

31. Briese M, et al. (2009) Deletion of *smn-1*, the *C. elegans* ortholog of the spinal muscular atrophy gene, results in locomotor dysfunction and reduced lifespan. *Hum Mol Genet* 18(11):97-104.

32. Dimitriadis M, et al. (2010) Conserved genes act as modifiers of invertebrate SMN loss of function defects. *PLoS Genet* 6(10):e1001172.

33. Avery L (1993) The genetics of feeding in *C. elegans*. *Genetics* 133(4):897-917.

34. Arribere JA, et al. (2014) Efficient marker-free recovery of custom genetic modifications with CRISPR/Cas9 in *Caenorhabditis elegans*. *Genetics* 198(3):837-846.

35. Friedland AE, et al. (2013) Heritable genome editing in *C. elegans* via a CRISPR-Cas9 system. *Nat Methods* 10(8):741-743.

36. Miguel-Aliaga I, et al. (1999) The *C. elegans* orthologue of the human gene responsible for spinal muscular atrophy is a maternal product critical for germline maturation and embryonic viability. *Hum Mol Genet* 8(12):2133-2143.

37. Monani UR & De Vivo DC (2014) Neurodegeneration in spinal muscular atrophy: from disease phenotype and animal models to therapeutic strategies and beyond. *Future Neurol* 9(1):49-65.

38. Mahoney TR, Luo S, & Nonet ML (2006) Analysis of synaptic transmission in *Caenorhabditis elegans* using an aldicarb-sensitivity assay. *Nat Protoc* 1(4):1772-1777.

39. Firnhaber C & Hammarlund M (2013) Neuron-specific feeding RNAi in *C. elegans* and its use in a screen for essential genes required for GABA neuron function. *PLoS Genet* 9(11):e1003921.

40. Sleight JN, et al. (2011) A novel *Caenorhabditis elegans* allele, *smn-1(cb131)*, mimicking a mild form of spinal muscular atrophy, provides a convenient drug screening platform highlighting new and pre-approved compounds. *Hum Mol Genet* 20(2):245-260.

41. Lewis JA, Wu CH, Berg H, & Levine JH (1980) The genetics of levamisole resistance in the nematode *Caenorhabditis elegans*. *Genetics* 95(4):905-928.

42. Miller KG, et al. (1996) A genetic selection for *C. elegans* synaptic transmission mutants. *Proc Natl Acad Sci U S A* 93(22):12593-12598.

43. Schuske KR, et al. (2003) Endophilin is required for synaptic vesicle endocytosis by localizing synaptotagmin. *Neuron* 40(4):749-762.

44. Clayton EL & Cousin MA (2009) The molecular physiology of activity-dependent bulk endocytosis of synaptic vesicles. *J Neurochem* 111(4):901-914.

45. Ch'ng Q, Sieburth D, & Kaplan JM (2008) Profiling synaptic proteins identifies regulators of insulin secretion and lifespan. *PLoS Genet* 4(11):e1000283.

46. Sieburth D, et al. (2005) Systematic analysis of genes required for synapse structure and function. *Nature* 436(7050):510-517.

47. White JG, Southgate E, Thomson JN, & Brenner S (1976) The structure of the ventral nerve cord of *Caenorhabditis elegans*. *Philos Trans R Soc Lond B Biol Sci* 275(938):327-348.

48. Wang Y, et al. (2006) The C2H2 zinc-finger protein SYD-9 is a putative posttranscriptional regulator for synaptic transmission. *Proc Natl Acad Sci U S A* 103(27):10450-10455.

49. Grant B, et al. (2001) Evidence that RME-1, a conserved *C. elegans* EH-domain protein, functions in endocytic recycling. *Nat Cell Biol* 3(6):573-579.

50. Fares H & Greenwald I (2001) Genetic analysis of endocytosis in *Caenorhabditis elegans*: coelomocyte uptake defective mutants. *Genetics* 159(1):133-145.

51. Cherry S & Perrimon N (2004) Entry is a rate-limiting step for viral infection in a *Drosophila melanogaster* model of pathogenesis. *Nat Immunol* 5(1):81-87.

52. Engel S, et al. (2011) Role of endosomes in simian virus 40 entry and infection. *J Virol* 85(9):4198-4211.

53. Pho MT, Ashok A, & Atwood WJ (2000) JC virus enters human glial cells by clathrin-dependent receptor-mediated endocytosis. *J Virol* 74(5):2288-2292.

54. Querbes W, O'Hara BA, Williams G, & Atwood WJ (2006) Invasion of host cells by JC virus identifies a novel role for caveolae in endosomal sorting of noncaveolar ligands. *J Virol* 80(19):9402-9413.

55. Dugan AS, Gasparovic ML, & Atwood WJ (2008) Direct correlation between sialic acid binding and infection of cells by two human polyomaviruses (JC virus and BK virus). *J Virol* 82(5):2560-2564.

56. Neu U, et al. (2010) Structure-function analysis of the human JC polyomavirus establishes the LSTc pentasaccharide as a functional receptor motif. *Cell Host & Microbe* 8(4):309-319.

57. Bevan AK, et al. (2010) Early heart failure in the SMNDelta7 model of spinal muscular atrophy and correction by postnatal scAAV9-SMN delivery. *Hum Mol Genet* 19(20):3895-3905.

58. Heier CR, Satta R, Lutz C, & DiDonato CJ (2010) Arrhythmia and cardiac defects are a feature of spinal muscular atrophy model mice. *Hum Mol Genet* 19(20):3906-3918.

59. Shababi M, et al. (2010) Cardiac defects contribute to the pathology of spinal muscular atrophy models. *Hum Mol Genet* 19(20):4059-4071.

60. Hua Y, et al. (2011) Peripheral SMN restoration is essential for long-term rescue of a severe spinal muscular atrophy mouse model. *Nature* 478(7367):123-126.

61. Somers E, et al. (2012) Density, calibre and ramification of muscle capillaries are altered in a mouse model of severe spinal muscular atrophy. *Neuromuscul Disord* 22(5):435-442.

62. Schreml J, et al. (2013) Severe SMA mice show organ impairment that cannot be rescued by therapy with the HDACi INJ-26481585. *Eur J Hum Genet* 21(6):643-652.

63. Bowerman M, et al. (2014) Defects in pancreatic development and glucose metabolism in SMN-depleted mice independent of canonical spinal muscular atrophy neuromuscular pathology. *Hum Mol Genet* 23(13): 3432-3444.

64. Allison AC (1954) Protection afforded by sickle-cell trait against subtertian malarial infection. *Br Med J* 1(4857):290-294.

65. Allison AC (1957) Malaria in carriers of the sickle-cell trait and in newborn children. *Exp Parasitol* 6(4):418-447.

66. Gabriel SE, et al. (1994) Cystic fibrosis heterozygote resistance to cholera toxin in the cystic fibrosis mouse model. *Science* 266(5182):107-109.

67. Lightfield KL, et al. (2008) Critical function for Naip5 in inflammasome activation by a conserved carboxy-terminal domain of flagellin. *Nat Immunol* 9(10):1171-1178.

68. Rage F, et al. (2013) Genome-wide identification of mRNAs associated with the protein SMN whose depletion decreases their axonal localization. *RNA* 19(12):1755-1766.

69. Zhang Z, et al. (2008) SMN deficiency causes tissue-specific perturbations in the repertoire of snRNAs and widespread defects in splicing. *Cell* 133(4):585-600.

70. Peter CJ, et al. (2011) The COPI vesicle complex binds and moves with survival motor neuron within axons. *Hum Mol Genet* 20(9):1701-1711.

71. Razi M, Chan EY, & Tooze SA (2009) Early endosomes and endosomal coatomer are required for autophagy. *J Cell Biol* 185(2):305-321.

72. Ting CH, et al. (2011) The spinal muscular atrophy disease protein SMN is linked to the Golgi network. *PLoS One* 7(12):e51826.

73. Oprea GE, et al. (2008) Plastin 3 is a protective modifier of autosomal recessive spinal muscular atrophy. *Science* 320(5875):524-527.

74. Kubler E & Riezman H (1993) Actin and fimbrin are required for the internalization step of endocytosis in yeast. *EMBO J* 12(7):2855-2862.

75. Hagiwara M, et al. (2011) Interaction of activated Rab5 with actin-bundling proteins, L- and T-plastin and its relevance to endocytic functions in mammalian cells. *Biochem Biophys Res Commun* 407(3):615-619.

76. Boulant S, et al. (2011) Actin dynamics counteract membrane tension during clathrin-mediated endocytosis. *Nat Cell Biol* 13(9):1124-1131.

77. Collins A, Warrington A, Taylor KA, & Svitkina T (2011) Structural organization of the actin cytoskeleton at sites of clathrin-mediated endocytosis. *Curr Biol* 21(14):1167-1175.

78. Sirotkin V (2011) Cell biology: actin keeps endocytosis on a short leash. *Curr Biol* 21(14):R552-554.

79. Giorgini F & Steiner JR (2013) Rab11 as a modulator of synaptic transmission. *Commun Integr Biol* 6(6):e26807.

80. Urwin H, et al. (2010) Disruption of endocytic trafficking in frontotemporal dementia with CHMP2B mutations. *Hum Mol Genet* 19(11):2228-2238.

81. Farg MA, et al. (2014) C9ORF72, implicated in amyotrophic lateral sclerosis and frontotemporal dementia, regulates endosomal trafficking. *Hum Mol Genet*.

82. Neveling K, et al. (2013) Mutations in BICD2, which encodes a golgin and important motor adaptor, cause congenital autosomal-dominant spinal muscular atrophy. *Am J Hum Genet* 92(6):946-954.

83. Li X, et al. (2010) Bicaudal-D binds clathrin heavy chain to promote its transport and augments synaptic vesicle recycling. *EMBO J* 29(5):992-1006.

84. Brenner S (1974) The genetics of *Caenorhabditis elegans*. *Genetics* 77(1):71-94.

85. Frokjaer-Jensen C, Davis MW, Ailion M, & Jorgensen EM (2012) Improved Mos1-mediated transgenesis in *C. elegans*. *Nat Methods* 9(2):117-118.

86. Frokjaer-Jensen C, et al. (2008) Single-copy insertion of transgenes in *Caenorhabditis elegans*. *Nat Genet* 40(11):1375-1383.

87. Sato K, et al. (2009) Differential requirements for clathrin in receptor-mediated endocytosis and maintenance of synaptic vesicle pools. *Proc Natl Acad Sci U S A* 106(4):1139-1144.

88. Kim JS, et al. (2008) A chemical-genetic strategy reveals distinct temporal requirements for SAD-1 kinase in neuronal polarization and synapse formation. *Neural Dev* 3:23.

89. Hall DH, Hartwig E, & Nguyen KC (2012) Modern electron microscopy methods for *C. elegans*. *Methods Cell Biol* 107:93-149.

90. Cardona A, et al. (2012) TrakEM2 software for neural circuit reconstruction. *PLoS One* 7(6):e38011.

91. Major EO, et al. (1985) Establishment of a line of human fetal glial cells that supports JC virus multiplication. *Proc Natl Acad Sci U S A* 82(4):1257-1261.

92. Vacante DA, Traub R, & Major EO (1989) Extension of JC virus host range to monkey cells by insertion of a simian virus 40 enhancer into the JC virus regulatory region. *Virology* 170(2):353-361.

93. Atwood WJ, et al. (1995) Evaluation of the role of cytokine activation in the multiplication of JC virus (JCV) in human fetal glial cells. *J Neurovirol* 1(1):40-49.

94. Kennedy S, Wang D, & Ruvkun G (2004) A conserved siRNA-degrading RNase negatively regulates RNA interference in *C. elegans*. *Nature* 427(6975): 645-649.

95. Firnhaber C & Hammarlund M (2013) Neuron-specific feeding RNAi in *C. elegans* and its use in a screen for essential genes required for GABA neuron function. *PLoS Genet* 9(11): e1003921.

96. Kamath RS & Ahringer J (2003) Genome-wide RNAi screening in *Caenorhabditis elegans*. *Methods* 30(4): 313-321.

97. Fares H & Greenwald I (2001) Genetic analysis of endocytosis in *Caenorhabditis elegans*: coelomocyte uptake defective mutants. *Genetics* 159(1): 133-145.

98. van Swinderen B, et al. (2001) Goalpha regulates volatile anesthetic action in *Caenorhabditis elegans*. *Genetics* 158(2): 643-655.

99. Clark SG, et al. (1997) A dynamin GTPase mutation causes a rapid and reversible temperature-inducible locomotion defect in *C. elegans*. *Proc Natl Acad Sci U S A* 94(19): 10438-10443.

1293
1294
1295
1296
1297
1298
1299
1300
1301
1302
1303
1304
1305
1306
1307
1308
1309
1310
1311
1312
1313
1314
1315
1316
1317
1318
1319
1320
1321
1322
1323
1324
1325
1326
1327
1328
1329
1330
1331
1332
1333
1334
1335
1336
1337
1338
1339
1340
1341
1342
1343
1344
1345
1346
1347
1348
1349
1350
1351
1352
1353
1354
1355
1356
1357
1358
1359
1360